Title: 222Rn and 220Rn concentrations in soil gas of the Izera Massif (Sudetes, Poland) as a function of sampling depth

Author: Dariusz Malczewski, Jerzy Żaba

Citation style: Malczewski Dariusz, Żaba Jerzy. (2017). 222Rn and 220Rn concentrations in soil gas of the Izera Massif (Sudetes, Poland) as a function of sampling depth. "Geological Quarterly" (Vol. 61, no. 4 (2017), s. 877-886), doi 10.7306/gq.1377

Geological Quarterly, 2017, **61** (4): 877–886
DOI: http://dx.doi.org/10.7306/gq.1377

^{222}Rn and ^{220}Rn concentrations in soil gas of the Izera Massif (Sudetes, Poland) as a function of sampling depth

Dariusz MALCZEWSKI[1,] * and Jerzy ŻABA[1]

[1] University of Silesia, Faculty of Earth Sciences, Będzińska 60, 41-200 Sosnowiec, Poland

Malczewski, D., Żaba, J., 2017. ^{222}Rn and ^{220}Rn concentrations in soil gas of the Izera Massif (Sudetes, Poland) as a function of sampling depth. Geological Quarterly, **61** (4): 877–886, doi: 10.7306/gq.1377

This research presents soil gas ^{222}Rn and ^{220}Rn concentrations measured at 17 locations in the Izera Massif of southwest Poland. The average ^{222}Rn concentrations at sampling depths of 10, 40 and 80 cm were 8, 78 and 224 kBq m^{-3}, respectively. The average ^{220}Rn concentrations for the same depths (10, 40 and 80 cm) were 6, 10 and 13 kBq m^{-3}, respectively. Profiles of the concentrations *versus* depth can be fitted by exponential, linear and polynomial functions for soils developed on fault zones, above uranium mineral deposits, and above faulted uranium deposits, respectively. Soils developed on bedrock without fault zones or uranium mineralisation exhibit concentrations that follow a power function with an exponent of p <1.

Key words: radon and thoron, fault zones, uranium mineralisation, Izera Massif.

INTRODUCTION

The Izera Massif is located in the Sudetic Block (southwestern Poland; Fig. 1) and is part of the Izera-Karkonosze Massif. The central part of the Izera-Karkonosze Massif consists of the Variscan-aged Karkonosze granite pluton (Karkonosze Massif; Fig. 1) while surrounding areas are composed of older metamorphic rocks. The Izera Massif forms the northern envelope of the Karkonosze granite pluton. The massif records extensive lateral evidence of both thermal and metasomatic contact metamorphism. The Intra-Sudetic Fault Zone runs along the northern border of the Izera Massif. To the west, the Izera Massif borders the neighbouring Lusatian Massif.

The radon isotopes ^{222}Rn (referred to as "radon", $T_{1/2}$ = 3.82 d) and ^{220}Rn (referred to as "thoron", $T_{1/2}$ = 55.6 s) belong to the ^{238}U and ^{232}Th decay series and occur as inert, radioactive gases. The mechanism by which ^{222}Rn and ^{220}Rn diffuses from minerals, soil and other regolith is not fully understood (Neznal et al., 1996; Ishimori et al., 2013; Malczewski and Dziurowicz, 2015). Atmospheric ^{222}Rn concentrations normally range from 4 to 19 Bq m^{-3}, whereas soil ^{222}Rn concentrations vary between ~4 and 40 kBq m^{-3} (Eisenbud and Gesell, 1997).

Malczewski and Żaba (2007) presented a comprehensive survey of radon and thoron concentrations in soil gas of the Izera-Karkonosze Massif. The present contribution reports and interprets the relationship between Rn isotope concentrations and sampling depths within soils developed in association with fault zones and uranium mineralisation. This paper also compares ^{222}Rn concentrations measured at 80 cm depth with results obtained by previous studies of the Izera Massif (e.g., Wołkowicz, 2007).

GEOLOGICAL SETTING

The Izera Massif consists mainly of gneisses, granite-gneisses, granites, granodiorites, leucogneisses, leucogranites and mica schists. Hornfelses, leptinites, greisens, skarns, erlans, amphibolites, quartzites and quartz veins are rare but present. The Izera granites were emplaced by Early Paleozoic (Cambrian to Ordovician) magmatism. The granites, granodiorites and gneisses from the eastern part of the Izera Massif have been dated using several different methods and span a general age range of 550–460 Ma (Borkowska et al., 1980; Jarmołowicz-Szulc, 1984; Korytowski et al., 1993; Kröner et al., 2001).

The Izera gneisses are thought to be a polygenic group. Most were formed by deformation of the Izera granite (Oberc-Dziedzic et al., 2005). The orthogneisses are mainly flaser gneisses and flaser-augen gneisses. Their deformation occurred over multiple episodes from the Early Paleozoic to the Pennsylvanian. A subset of gneisses including laminated gneisses or laminated augen gneisses probably reflects metamorphism of Neoproterozoic supracrustal series (Żaba, 1984). The protoliths were Neoproterozoic pelites such as clay rocks and mudstones. Mica-schists (supracrustal series) envelop the intrusive Izera granites (Oberc-Dziedzic et al., 2005) and form four parallel belts (Fig. 1). Mica-schists were metamorphosed at greenstone or amphibolite facies (Żaba, 1985; Cook and Dudek, 1994). Mica-schists from the Szklarska Poręba belt and from part of the Stara Kamienica belt have been metamorphosed to cordierite-andalusite-biotite hornfelses.

* Corresponding author, e-mail: dariusz.malczewski@us.edu.pl
Received: April 27, 2017; accepted: July 18, 2017; first published online: September 11, 2017

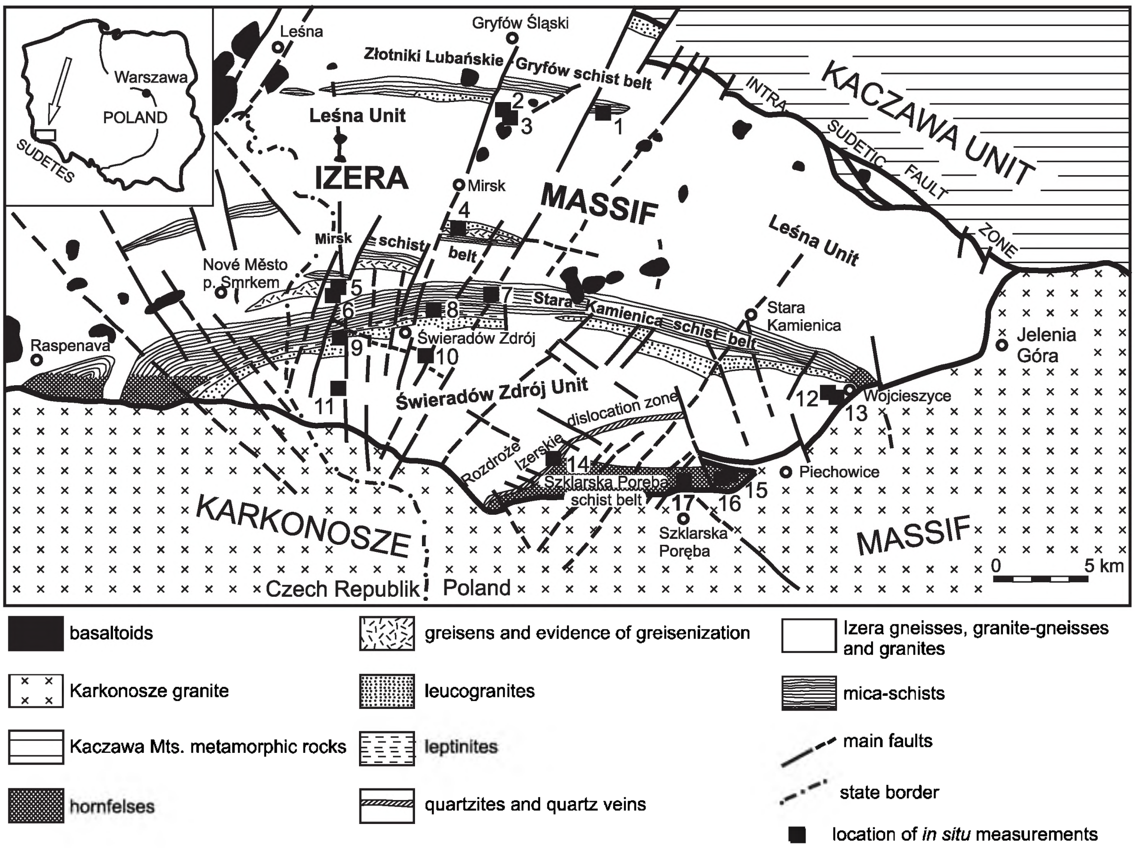

Fig. 1. Geological map of the Izera Massif area, showing measurement locations

1–17 – locations of *in situ* measurements

The Izera Massif formations experienced several episodes of deformation (Żaba and Teper, 1989; Mierzejewski and Oberc-Dziedzic, 1990; Mazur and Kryza, 1996). The Izera Massif is cut by numerous faults running E–W, NW–SE, N–S and NE–SW (Fig. 1). The oldest E–W-trending faults frequently formed in association with the schist belts and generally run parallel to them. Multiphase fault-related activity and associated metasomatic processes (Smulikowski, 1972; Kozłowski, 1974; Żaba, 1984) resulted in the formation of leucogneisses, leucogranites and leptinites (Fig. 1). Metasomatic processes have produced several different varieties of greisen (Fig. 1), which commonly exhibit ore-bearing mineralisation. Polymetallic mineralisation also occurs within the Stara Kamienica schist belt (Cook and Dudek, 1994; Mochnacka et al., 2015). Uranium and thorium mineralisation occurs throughout the Izera Massif (Mochnacka and Banaś, 2000).

MATERIALS AND METHODS

Measurements of soil ^{222}Rn and ^{220}Rn concentrations were performed using a RAD7 portable radon analysis system (Fig. 2). The detector operates with a sensitivity of 4 Bq m^{-3} and an upper linear detection limit of 800 kBq m^{-3}. The upper range can be increased using a peripheral device. After inserting the stainless steel probe at the specified sampling depth (10, 40 and 80 cm), the sampling outlet was connected to the inlet of the RAD7 via a drying tube. The soil gas measurements were carried out in sniff mode. In this mode, the built-in pump runs continuously and ^{222}Rn and ^{220}Rn concentrations are calculated from the data in electronic windows A and B, respectively. The cycle time was 15 min and three cycles were performed for all measurements. An average of these three cycles provided results reported for a given depth. Before each measurement, the RAD7 was purged for at least 10 min, or longer if the previous analysis detected high radon and thoron concentrations. Figure 3 shows sampling locations described in Table 1.

RESULTS AND DISCUSSION

Tables 2 through 5 report parameters derived from fitting ^{222}Rn and ^{220}Rn data to sampling depths. All of the fitting parameters are valid for sampling depths in the range of 10 to 80 cm.

Fig. 2. The 16, 46 and 100 cm gas probes and RAD7 detector

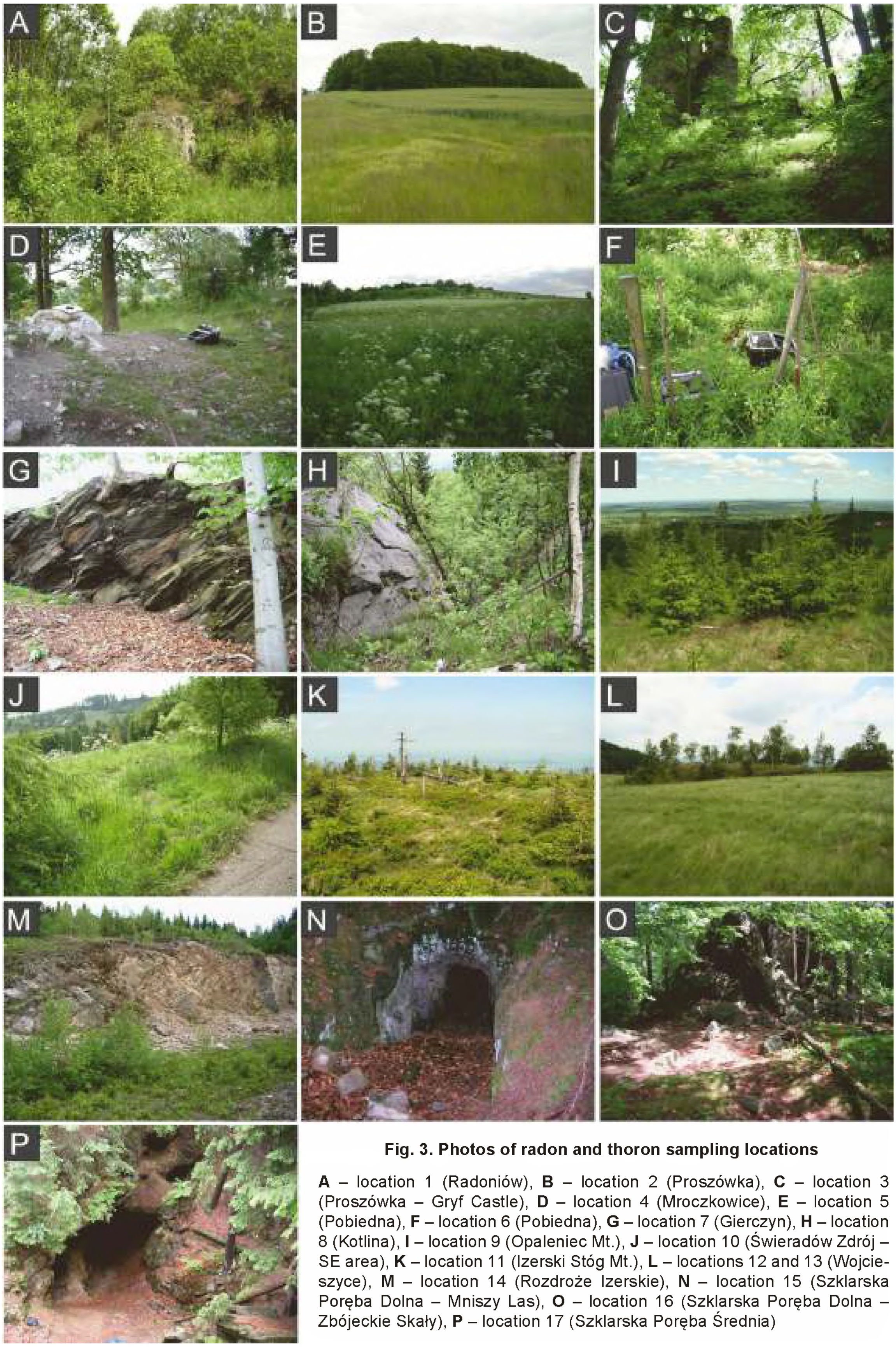

Fig. 3. Photos of radon and thoron sampling locations

A – location 1 (Radoniów), **B** – location 2 (Proszówka), **C** – location 3 (Proszówka – Gryf Castle), **D** – location 4 (Mroczkowice), **E** – location 5 (Pobiedna), **F** – location 6 (Pobiedna), **G** – location 7 (Gierczyn), **H** – location 8 (Kotlina), **I** – location 9 (Opaleniec Mt.), **J** – location 10 (Świeradów Zdrój – SE area), **K** – location 11 (Izerski Stóg Mt.), **L** – locations 12 and 13 (Wojcieszyce), **M** – location 14 (Rozdroże Izerskie), **N** – location 15 (Szklarska Poręba Dolna – Mniszy Las), **O** – location 16 (Szklarska Poręba Dolna – Zbójeckie Skały), **P** – location 17 (Szklarska Poręba Średnia)

Table 1

Location of *in situ* measurements

No.	Location	Rocks	Tectonics
1.	Radoniów – closed uranium mine	Fine-grained augen gneisses with granite-gneisses, leucogneisses, leucogranites, leptinites, mica-schists and amphibolites	
2.	Proszówka	Augen gneisses	NE–SW-trending fault nearby
3.	Proszówka – Gryf Castle	Contact between Cenozoic basalts and augen gneisses	Volcanic features in the area follow a NE–SW-trending fault zone
4.	Mroczkowice near Mirsk – Wyrwak Hill	Greisens	WNW–ESE-trending fault zone running parallel along the northern border of the Mirsk schist belt
5.	Pobiedna – closed uranium mine	Augen gneisses with symptoms greisenization	Fault zones trending N–S and NE–SW, creating a distinct tectonic loop in the area
6.	Pobiedna – old uranium prospecting drift	Augen gneisses and granite-gneisses	Region cut by a NE–SW-trending fault zone
7.	Gierczyn – Blizbor Hill	Mica-schists (ore-bearing mineralisation)	
8.	Kotlina	Leptinites	The leptinites follow an old E–W-trending fault zone, running along the southern border of the Stara Kamienica schist belt
9.	Świeradów Zdrój (Czerniawa) – Opaleniec Mt.	Leucogranites	Units near two fault zones: an older E–W-trending fault zone along the southern border of the Stara Kamienica schist belt and a slightly younger N–S-trending fault zone
10.	Świeradów Zdrój – SE area	Laminated augen gneisses	Gneisses occur at the intersection of a WNW–ESE-trending fault and a slightly younger NE–SW fault zone
11.	Izerski Stóg Mt.	Fine-grained flaser-augen gneisses	Area cut by a distinct N–S fault zone
12.	Wojcieszyce – closed uranium mine	Augen gneisses and granite-gneisses	Contact zone of the Variscan Karkonosze granites
13.	Wojcieszyce – closed uranium mine	Augen gneisses	Contact zone of the Variscan Karkonosze granites
14.	Rozdroże Izerskie – closed quarry	Quartz vein	The fault zone runs NE–SW; zone cut by numerous younger, transverse, NW–SE trending faults
15.	Szklarska Poręba Dolna – Mniszy Las	Hornfelses	Contact zone of the Variscan Karkonosze granites
16.	Szklarska Poręba Dolna – Zbójeckie Skały	Hornfelses	Contact zone of the Variscan Karkonosze granites
17.	Szklarska Poręba Średnia	Hornfelses	Contact zone of the Variscan Karkonosze granites

Table 2

Fitted parameters for the exponential function given by Eq. [1] (see text)

Location	^{222}Rn		
	A	b	C_{80} (kBq m^{-3})
9	10	0.123	186.0 ±5.2
10	149	0.087	157.0 ±4.6
11	182	0.092	282.0 ±7.1
Location	^{220}Rn		
9	0.581	0.135	29.2 ±4.2
11	653	0.043	20.4 ±2.8

Uncertainties estimated for parameters are ≤10%; C_{80} refers to the average activity concentrations of ^{222}Rn and ^{220}Rn at 80 cm depth

CONCENTRATIONS OF ^{222}Rn AND ^{220}Rn IN SOILS DEVELOPED WITHIN FAULT ZONES

Sampling points located within fault zones (locations 9–11) showed exponential dependence of ^{222}Rn on sampling depth (Fig. 4). The same pattern was also observed for ^{220}Rn at locations 9 and 11 (Fig. 4). Concentration vs. depth profiles can be described by the exponential function:

$$C_{222/220}(\text{Bq m}^{-3}) = A \exp (b \cdot d) \quad [1]$$

where: d is the depth (cm).

Table 2 lists calculated values for A, b and the ^{222}Rn and ^{220}Rn concentrations at a depth of 80 cm. Concentrations of ^{220}Rn at location 10 do not adhere to Eq. [1] because the sample location occurred on a steep slope. For slope sample locations, ^{220}Rn concentration showed a pronounced inverse relationship with depth whereby the concentration significantly decreased with increasing depth (Malczewski and Żaba, 2007). As shown in Table 2, location 9 (Opaleniec Mt.) gave the highest b term values for both ^{222}Rn and ^{220}Rn (0.123 and 0.135, respectively). The highest ^{222}Rn concentration (282 kBq m^{-3}) was recorded at location 11, whereas the highest ^{220}Rn concentration (29 kBq m^{-3}) was recorded at location 9 (Table 2). Enhanced radon flux has been interpreted as an indicator of active fault zones since the 1970s. King (1978) reported an exponential trend of radon concentration vs. depth on the San Andreas Fault.

Neznal et al. (1996) reported the highest values of ^{222}Rn concentrations among the sampling points, reaching 100–120 kBq m^{-3}. These values occurred in soils at a depth of 80 cm at locations in the test area (Chaby area, Prague, the

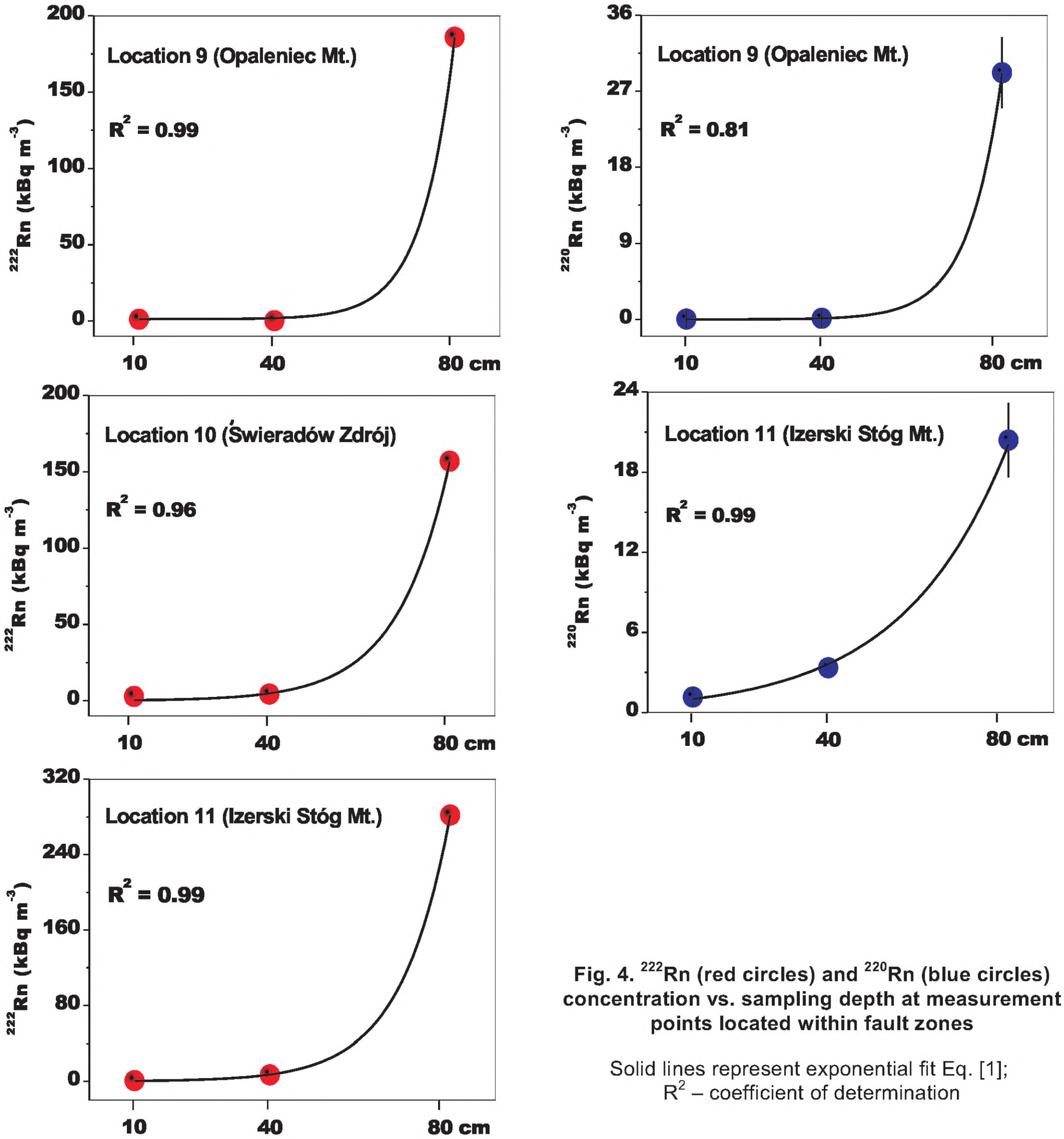

Fig. 4. **^{222}Rn (red circles) and ^{220}Rn (blue circles) concentration vs. sampling depth at measurement points located within fault zones**

Solid lines represent exponential fit Eq. [1]; R^2 – coefficient of determination

Czech Republic) where there are tectonic zones with transverse faults. Barnet and Pacherová (2015) recorded average values of ^{222}Rn concentrations that ranged from 12 to 22 kBq m^{-3} and 18 to 60 kBq m^{-3} in sites located in contact zones (granitoids or migmatites with sandstones, and trachytes with Cretaceous sediments; Klatovy, Kytlice, Veseli nad Lužnici and Chrudim areas, the Czech Republic) at depths of 50 and 80 cm, respectively. Al-Tamimi and Abumurad (2001) reported the soil radon concentrations that ranged from 25 to 60 kBq m^{-3} at 50 cm depth along faults in Wadi um Ghudram and Wadi Es-sir Formation (N Jordan).

Lower ^{222}Rn and ^{220}Rn soil gas concentrations than those presented here were reported by Al-Hamidawi et al. (2012) in the vicinity of Al-Kufa city (Iraq), which is cut by fault zones located in sandstones. They observed average ^{222}Rn concentrations of 3630, 4411 and 4717 Bq m^{-3}, and the ^{220}Rn concentrations of 13, 65, and 84 Bq m^{-3} at sampling depths of 50, 100 and 150 cm, respectively. Similar low values in the range of 29 to 7059 Bq m^{-3} at 50 cm depth were reported for soil radon measurements around fault lines in the western part of the north Anatolian fault zone (Turkey) by Yakut et al. (2017).

CONCENTRATIONS OF ^{222}Rn AND ^{220}Rn IN SOILS DEVELOPED ABOVE URANIUM DEPOSITS WITHOUT FAULT ZONES

Locations 1 and 12 represent known uranium deposits and exhibited linear relationships between ^{222}Rn concentrations and soil depth (Fig. 5). Location 1 also showed linear ^{220}Rn vs. depth relations (Fig. 5). This indicates that thorium follows a distribution similar to that of uranium at location 1. The ^{222}Rn concentration vs. depth relation at locations 1 and 12, and ^{220}Rn concentrations vs. depth at location 1 can be fitted by the linear expression:

$$C_{222/220}(\text{Bq m}^{-3}) = A + (b \cdot d) \qquad [2]$$

Table 3 lists calculated values for A and b along with ^{222}Rn and ^{220}Rn concentrations at 80 cm depth. As with location 10, location 12 also occurred along a slope and exhibited inverse ^{220}Rn concentration vs. depth relations. Similar ^{220}Rn concentration values at depths of 10, 40 and 80 cm from location 12 likely reflect interactions between inverse and linear influences on ^{220}Rn concentrations (Fig. 5).

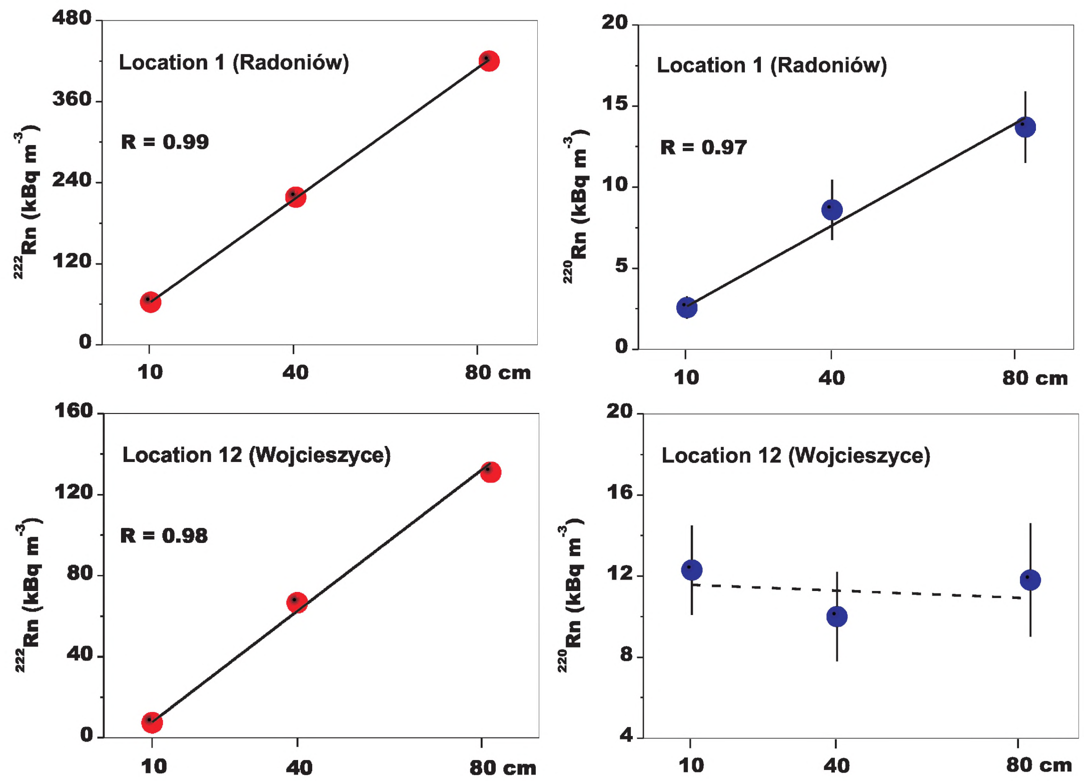

Fig. 5. ^{222}**Rn (red circles) and** ^{220}**Rn (blue circles) concentrations vs. sampling depth at measurement points located above uranium deposits**

Solid lines represent linear regressions – Eq. [2]; R – correlation coefficient

CONCENTRATIONS OF ^{222}Rn AND ^{220}Rn IN SOILS DEVELOPED ABOVE FAULT ZONES WITH URANIUM MINERALISATION

Locations 5 and 6 (600 m apart) were located in Pobiedna amid both fault zones and uranium deposits. At these sites, ^{222}Rn concentration vs. depth measurements can be fitted by a second order polynomial function (Fig. 6):

$$C_{222}\ (\text{Bq m}^{-3}) = A + (b_1 \cdot d) + (b_2 \cdot d^2) \qquad [3]$$

Table 4 lists calculated values for A, b_1, b_2 and the ^{222}Rn concentrations at 80 cm depth. As shown in Table 4, location 6 provided the highest ^{222}Rn concentration (~2.2 MBq m^{-3}) observed in the Izera Massif. The highest soil gas ^{222}Rn concentration was also recorded in Pobiedna (~7 MBq m^{-3}) during uranium ore prospecting activities from 1945–1954 (Solecki, 1997). The observed deviation from linearity (Fig. 6) probably results from enhanced gas flow along fault zones in the area (Malczewski and Żaba, 2007). Location 5 exhibited a similar polynomial depth dependence of ^{220}Rn (Fig. 6 and Table 4). Because the RAD7 counts became non-linear at 80 cm depth, the exact ^{220}Rn concentration at location 6 could not be determined.

Goodwin et al. (2008) measured soil gas ^{222}Rn concentrations that ranged from 0.1 to 207 kBq m^{-3} with a mean of 25 kBq m^{-3} at a depth of 60 cm. These values were obtained from 72 sampling points in Nova Scotia (Canada). Nova Scotia is characterized by areas of elevated background levels and occurrences of uranium. The same authors reported soil gas radon concentrations of 500 to 1500 kBq m^{-3} that were associated with the well-known Milet Brook uranium deposit. These values are similar to those presented here at locations 1 (Radoniów) and 6 (Pobiedna).

Table 3

Fitted parameters for the linear expression given by Eq. [2] (see text)

Location	^{222}Rn		
	A	b	C_{80} (kBq m^{-3})
1	11981	5126	420.0 ±10.6
12	–10552	1827	131.0 ±4.2
Location	^{220}Rn		
1	998	166	13.7 ±3.2

Uncertainties estimated for the parameters are ≤10%. C_{80} refers to the average activity concentrations of ^{222}Rn and ^{220}Rn at 80 cm depth

CONCENTRATIONS OF ^{222}Rn AND ^{220}Rn IN TYPICAL SOILS

In typical soils (without fault zones and/or uranium mineralisation) both the ^{222}Rn and ^{220}Rn concentrations vs. depth follow a power function:

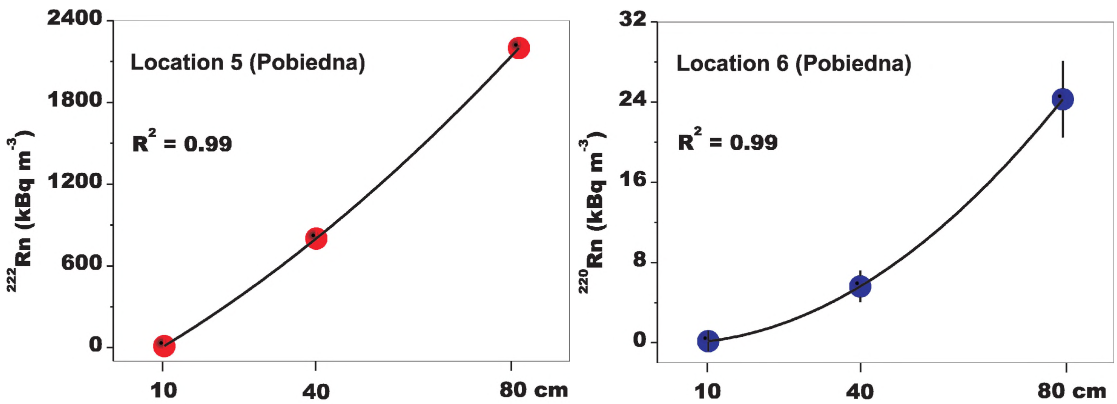

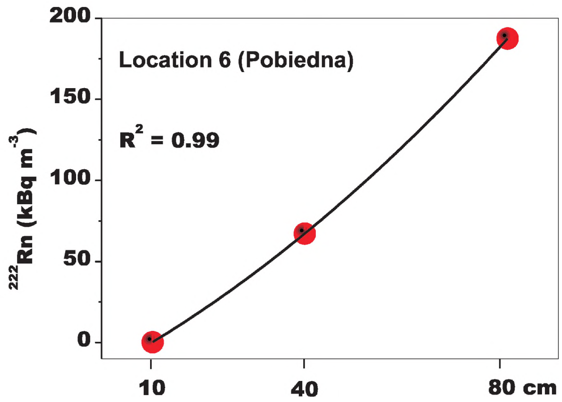

Fig. 6. ^{222}Rn (red circles) and ^{220}Rn (blue circles) concentrations vs. sampling depth at measurement points located above uranium deposits and fault zones

Solid lines represent polynomial regressions – Eq. [3]; R^2 – coefficient of determination

Table 4

Fitted parameters for the polynomial function given by Eq. [3] (see text)

Location	^{222}Rn			
	A	b_1	b_2	C_{80} (kBq m^{-3})
5	–202647	20149	5124	2200 ±22.6
6	–17604	1676	11	187.5 ±10.6
Location	^{220}Rn			
6	–47	–21	4.1	24.3 ±3.8

Uncertainties estimated for the parameters are ≤10%. C_{80} refers to the average activity concentrations of ^{222}Rn and ^{220}Rn at 80 cm depth

Table 5

Fitted parameters for the power function given by Eq. [4] (see text)

Location	^{222}Rn		
	A	p	C_{80} (kBq m^{-3})
4	2140	0.856	88.9 ±3.1
15	1798	0.640	27.4 ±1.5
Location	^{220}Rn		
4	3689	0.353	16.1 ±2.7
15	560	0.732	13.0 ±2.1

Uncertainties estimated for the parameters are ≤20%. C_{80} refers to the average activity concentrations of ^{222}Rn and ^{220}Rn at 80 cm depth

$$C_{222/220}(\text{Bq m}^{-3}) = A \times d^{p} \quad [4]$$

with the exponent $p < 1$ (Table 5). Figure 7 shows depth concentrations of ^{222}Rn and ^{220}Rn in soils developed on greisens (location 4) and hornfelses (location 15). As seen in Table 5, the calculated p value for ^{222}Rn at location 4 is noticeably higher than that calculated for ^{220}Rn. Location 15, however, gave comparable p values (within uncertainties).

Wang et al. (2016) reported average ^{222}Rn and ^{220}Rn concentrations of 130 and 188 kBq m^{-3}, respectively, at a depth of 80 cm in soils developed on weathered granite (S China). These values exceeded those obtained in our work at locations 4 and 15. For selected sites in the investigated area, the authors showed an almost exact logarithmic increase of ^{222}Rn concentrations with sampling depths from 20 to 160 cm at intervals of 20 cm. No rule was observed for the ^{220}Rn concentrations (Wang et al., 2016). Almayahi et al. (2013) obtained radon and thoron concentrations at a depth of 50 cm in Northern Peninsular Malaysia that ranged from 134 Bq m^{-3} to 143 kBq m^{-3}, and 55 to 423 Bq m^{-3}, respectively. The measurements were taken in soils mostly developed on granitic rocks, and the calculated average radon concentration was 29 kBq m^{-3} (Almayahi et al., 2013). Elzain (2017) has recently reported ^{222}Rn concentrations ranging from 4.2 to 15.2 kBq m^{-3} with an average of 9.1 kBq m^{-3} in soils formed mainly on basaltic rocks in the eastern part of Sudan. In the paper, the ^{222}Rn concentrations increased with sampling depth from 10 to 50 cm at intervals of 5 cm (Elzain, 2017).

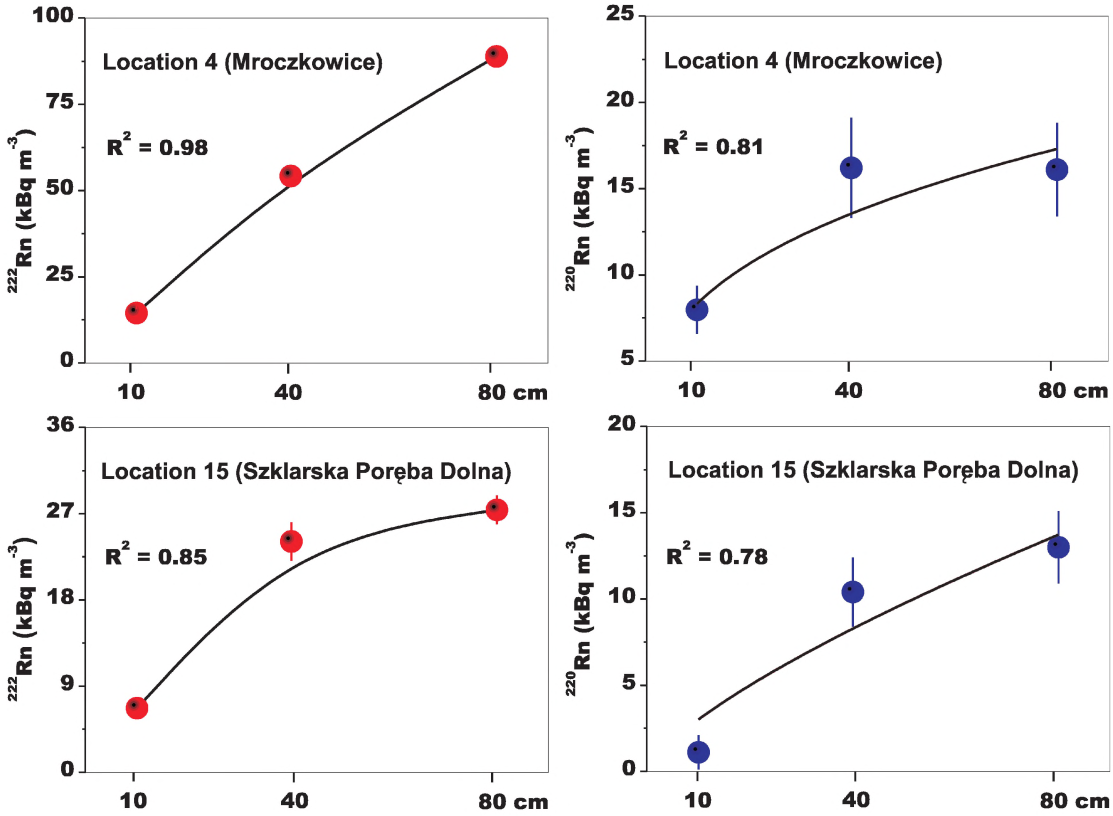

Fig. 7. ^{222}**Rn (red circles) and** ^{220}**Rn (blue circles) concentrations vs. sampling depth at measurement points located in typical soils (without uranium deposits or fault zones)**

Solid lines represent power function fits – Eq. [4]; R^2 – coefficient of determination

Similar to the fault zones, considerably lower values of ^{222}Rn concentrations were reported for soils developed on sandstones (Hasan et al., 2011; Alharbi and Abbady, 2013). Hasan et al. (2011) presented soil gas ^{222}Rn concentrations of 788, 1490, 2128 and 3273 Bq m^{-3} in the vicinity of Al-Najaf Al-Ashart city (Iraq) at depths of 5, 25, 35 and 60 cm, respectively. Alharbi and Abbady (2013) recorded average radon concentrations of 123, 163 and 220 Bq m^{-3} in the Al-Quassim area (Saudi Arabia) at depths of 20, 40 and 60 cm, respectively.

AVERAGE DEPTH CONCENTRATIONS OF ^{222}Rn AND ^{220}Rn IN SOILS FROM THE IZERA MASSIF

Figures 8 and 9 compare ^{222}Rn concentrations at 80 cm obtained by Malczewski and Żaba (2007) with those reported by Wołkowicz (2007). As seen in Figure 8, Wołkowicz (2007) reported average ^{222}Rn values nearly three times lower than values presented here. This discrepancy likely reflects the elevated radon concentrations observed in fault zones. Wołkowicz

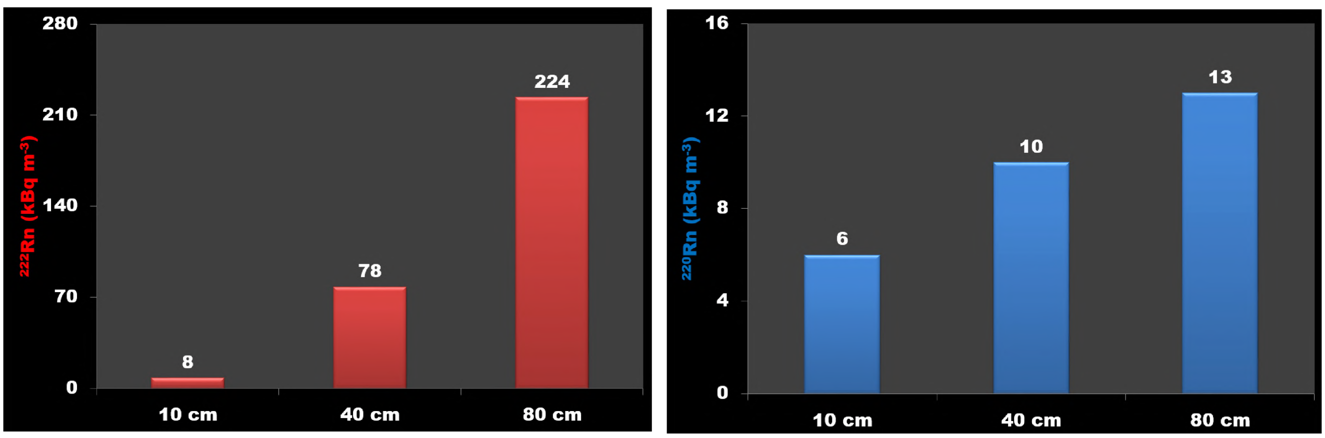

Fig. 8. **Average** ^{222}**Rn (red bars) and** ^{220}**Rn (blue bars) concentrations of soil gas in the Izera Massif at specified depths**

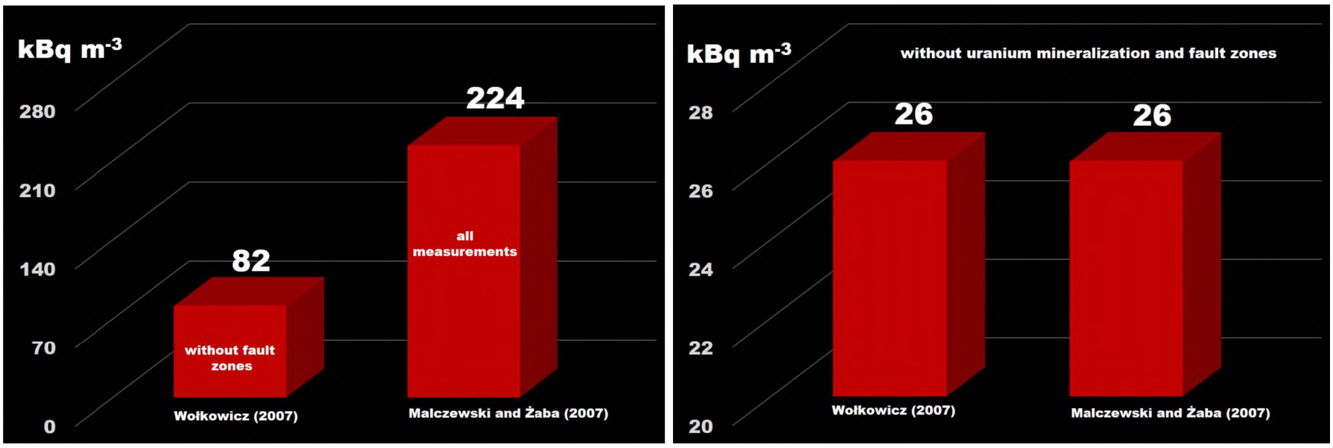

Fig. 9. Comparison of average ^{222}Rn concentrations at 80 cm depth calculated based on data reported by Wołkowicz (2007) and Malczewski and Żaba (2007)

Measurements by Wołkowicz (2007) avoided fault zones; standard deviations on the right-side graph are on the order of 20 kBq m^{-3}

(2007) avoided fault zones whereas this research did not. Results reported in Wołkowicz (2007) are consistent with those reported here, which were derived from locations without fault zones and uranium deposits (Fig. 9).

CONCLUSIONS

Results of ^{222}Rn and ^{220}Rn concentrations vs. depth in the Izera Massif have shown different patterns depending on the bedrock lithology, uranium mineralisation, and occurrence of fault zones. In soils developed above fault zones, a pronounced exponential relationship between ^{222}Rn concentrations and depth was observed. This relationship may characterize active fault zones. Excluding fault zones and uranium deposits, the average ^{222}Rn concentrations at 80 cm depth presented in this work resemble values reported for Izera Massif soils by previous research.

Acknowledgements. This work was supported by the National Science Centre, Poland, through grant No. 2014/15/B/ST10/04095. We thank S. Wołkowicz and A.T. Solecki for critical comments that improved the final version of this paper. The authors also thank T.M. Peryt for his help and editorial guidance.

REFERENCES

Al-Hamidawi, Ali, A., Jabar, Q.S., Al-Mashhadani, A.H., Al-Bayati, A.A., 2012. Measurement of radon and thoron concentrations of soil- gas in Al-Kufa city using RAD-7 detector. Iraqi Journal of Physics, **10**: 110–116.

Alharbi, W.R., Abbady, A.G.E., 2013. Measurement of radon concentrations in soil and the extent of their impact on the environment from Al-Qassim, Saudi Arabia. Natural Science, **5**: 93–98.

Almayahi, B.A., Tajuddin, A.A., Jaafar, M.S., 2013. *In situ* soil ^{222}Rn and ^{220}Rn and their relationship with meteorological parameters in tropical Northern Peninsular Malaysia. Radiation Physics and Chemistry, **90**: 11–20.

Al-Tamimi, M.H., Abumurad, K.M., 2001. Radon anomalies along faults in North of Jordan. Radiation Measurements, **34**: 397–400.

Barnet, I., Pacherová, P., 2015. The influence of rock contacts on the soil gas radon concentration and gamma dose rate. Geoscience Research Reports, **48**: 75–78.

Borkowska, M., Hameurt, J., Vidal, P., 1980. Origin and age of Izera granite and Rumburk granite in the Western Sudetes. Acta Geologica Polonica, **30**: 121–146.

Cook, N.J., Dudek, K., 1994. Mineral chemistry and metamorphism of garnet-chlorite-mica schists associated with cassiterite-sulphide-mineralisation from the Kamienica Range, Izera Mountains, SW Poland. Chemie der Erde, **54**: 1–32.

Eisenbud, M., Gesell, T., 1997. Environmental Radioactivity from Natural, Industrial, and Military Sources. Academic Press, San Diego.

Elzain, A.E.A., 2017. Determination of soil gas radon concentration from some locations of Gedarif town, Sudan by using CR-39. Radiation Protection, **32**: 85–90.

Goodwin, T.A., Ford, K.L., Friske, P.W.B., McIsaac, E.M., 2008. Radon soil gas in Nova Scotia. In: Mineral Resources Branch, Report of Activities 2008; Nova Scotia Department of Natural Resources, Report ME 2009-1: 25–34.

Hasan, A.K., Subber, A.R.H., Shaltakh, A.R., 2011. Measurement of radon concentration in soil gas using RAD7 in the environs of Al-Najaf Al-Ashraf City-Iraq. Advances in Applied Science Research, **22**: 273–278.

Ishimori, Y., Lange, K., Martin, P., Mayya, Y.S., Phaneuf, M., 2013. Measurement and calculation of radon releases from NORM residues. Technical Reports Series, 474. International Atomic Energy Agency, Vienna.

Jarmołowicz-Szulc, K., 1984. Geochronological study of a part of the northern cover of the Karkonosze Granite by fission track methods. Archiwum Mineralogiczne, **39**: 139–183.

King, C.Y., 1978. Radon emanation on San Andreas Fault. Nature, **271**: 516–519.

Korytowski, A., Dörr, W., Żelaźniewicz, A., 1993. U-Pb dating of metagranitoids in the NW Sudetes (Poland) and their bearing on tectonostratigraphic correlation. Terra Nova, **5**: 331–332.

Kozłowski, K., 1974. Crystalline schists and leucogranites of the Stara Kamienica–Świeradów Zdrój Belt (Western Sudetes). Geologia Sudetica, **9**: 7–98.

Kröner, A., Jaeckel, P., Hegner, E., Opletal, M., 2001. Single zircon ages and whole-rock Nd isotopic systematics of early Palaeozoic granitoid gneisses from the Czech and Polish Sudetes (Jizerské hory, Krkonoše and Orlice-Sněžik Complex). International Journal of Earth Sciences, **90**: 304–324.

Malczewski, D., Dziurowicz, M., 2015. ^{222}Rn and ^{220}Rn emanations as a function of the absorbed a-doses from select metamict minerals. American Mineralogist, **100**: 1378–1385.

Malczewski, D., Żaba, J., 2007. ^{222}Rn and ^{220}Rn concentrations in soil gas of Karkonosze-Izera Block (Sudetes, Poland). Journal of Environmental Radioactivity, **92**: 144–164.

Mazur, S., Kryza, R., 1996. Superimposed compressional and extensional tectonics in the Karkonosze-Izera Block, NE Bohemian Massif. In: Basement Tectonics, **11** (Europe and Other Regions) (eds. O. Oncken and C. Janssen): 51–66. Kluwer, Potsdam-Dordrecht.

Mierzejewski, M.P., Oberc-Dziedzic, T., 1990. The Izera-Karkonosze Block and its tectonic development (Sudetes, Poland). Neues Jahrbuch für Geologie und Paläontologie, Abhandlungen, **179**: 197–222.

Mochnacka, K., Banaś, M., 2000. Occurrence and genetic relationships of uranium and thorium mineralization in the Karkonosze-Izera Block (the Sudety Mts., SW Poland). Annales Societatis Geologorum Poloniae, **70**: 137–150.

Mochnacka, K., Oberc-Dziedzic, T., Mayer, W., Pieczka, A., 2015. Ore mineralization related to geological evolution of the Karkonosze-Izera Massif (the Sudetes, Poland) – towards a model. Ore Geology Reviews, **64**: 215–238.

Neznal, M., Neznal, M., Šmerda, J., 1996. Assessment of radon potential of soils: a five-year experience. Environment International, **22** (Suppl. 1): s819–s828.

Oberc-Dziedzic, T., Pin, C., Kryza R., 2005. Geodynamic setting of the Early Palaeozoic granitoid magmatism in the Variscides: Sm-Nd constrains from the Izera granitogneisses (W Sudetes, SW Poland). International Journal of Earth Sciences, **94**: 354–368.

Smulikowski, W., 1972. Petrogenetic and structural problems of the northern cover of the Karkonosze granite. Geologia Sudetica, **6**: 97–188.

Solecki, A.T., 1997. Radon geochemistry. In: XVII Szkoła Jesienna Polskiego Towarzystwa Badań Radiacyjnych im. Marii Skłodowskiej Curie (in Polish): 124–154. 22–26 September 1997, Zakopane.

Wang, M., Zheng, L., Chu, X., Li, S., Yan, S., 2016. The characteristics of radon and thoron concentration from soil gas in Shenzhen City of Southern China. Nukleonika, **61**: 305–309.

Wołkowicz, S., 2007. Radon potential of Sudetes and selected units of Fore-Sudetic Block. In: Radon Potential of Sudetes with Determination of Potentially Medicinal Radon Water Areas (ed. S. Wołkowicz) (in Polish with English summary): 5–107. Państwowy Instytut Geologiczny, Warszawa.

Yakut, H., Tabar, E., Yildirim, E., Zenginerler, Z., Ertugral, F., Demirci, N., 2017. Soil gas radon measurements around fault lines on the western section of the north Anatolian fault zone in Turkey. Radiation Protection Dosimetry, **173**: 405–413.

Żaba, J., 1984. Genesis and metamorphic evolution of gneisses and granitoids of the Izerski Stóg massif, Western Sudetes (in Polish with English summary). Geologia Sudetica, **19**: 89–190.

Żaba, J., 1985. Progressive regional metamorphism of the Izera Block, Western Sudetes (Poland). Acta Universitas Carolinae, Geologica, **1**: 63–88.

Żaba, J., Teper, L., 1989. Tectonic transport directions in the Izera Block, Western Sudeten. Krystalinikum, **20**: 131–150.